Supplementary information

Operando spectroscopic ellipsometry enables direct quantification of dynamic degradation rates in photoelectrochemical cells

Jiri Kollmann[1], Mauricio Schieda[1*], Ragle Raudsepp[1], Sehun Seo[1], Thomas Klassen[2,3] & Francesca Maria Toma[1,3,4,5*]

[1] Institute of Functional Materials for Sustainability, Helmholtz-Zentrum Hereon GmbH, Kantstr. 55, Teltow 14513, Germany.

[2] Institute of Hydrogen Technology, Helmholtz-Zentrum Hereon GmbH, Max-Planck-Str. 1, Geesthacht 21502, Germany.

[3] University of the Federal Armed Forces, Helmut-Schmidt-University, Holstenhofweg 85, Hamburg 22043, Germany.

[4] Chemical Sciences Division, Lawrence Berkeley National Lab, 1 Cyclotron Road, 94720, Berkeley 94720, California, USA

[5] Liquid Sunlight Alliance, Lawrence Berkeley National Laboratory, 1 Cyclotron Road, 94720, Berkeley 94720, California, USA

***email: francesca.toma@hereon.de; mauricio.schieda@hereon.de**

Contents

Experimental setup for *operando*-SE

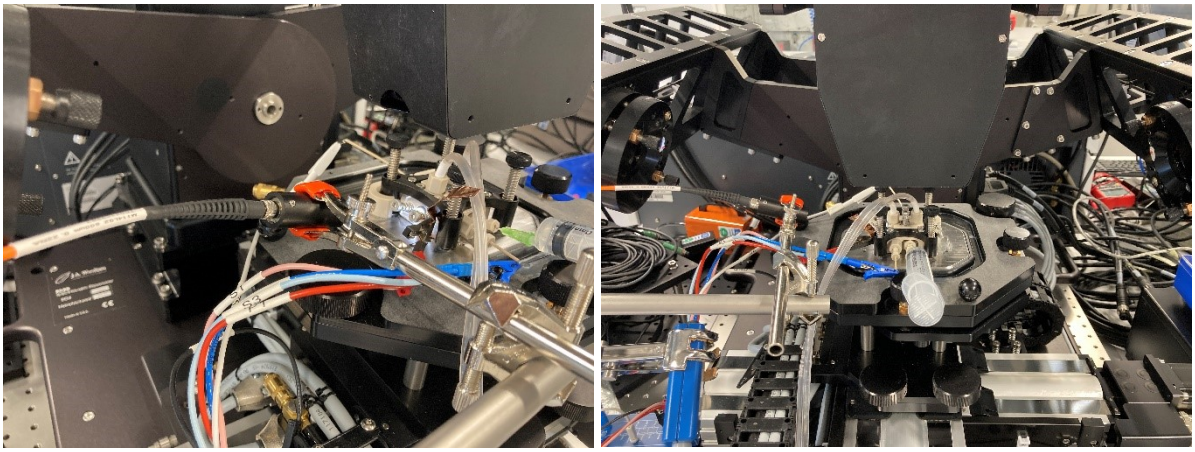

Supplementary Fig. S1. Liquid cell stage configuration used for *operando*-spectroscopic ellipsometry (SE) at a fixed angle of 70°. Simulated sunlight or UV light is introduced into the photoelectrochemical (PEC) cell using a solarization-resistant fiber optic cable with a core diameter of 600 µm and a numerical aperture of 0.22 for lateral illumination of the sample under photoelectrochemical operating conditions.

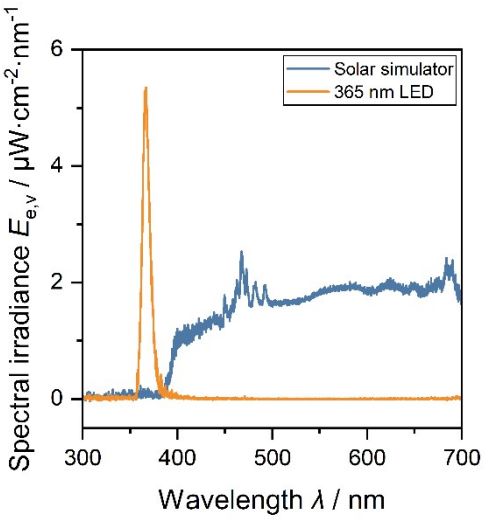

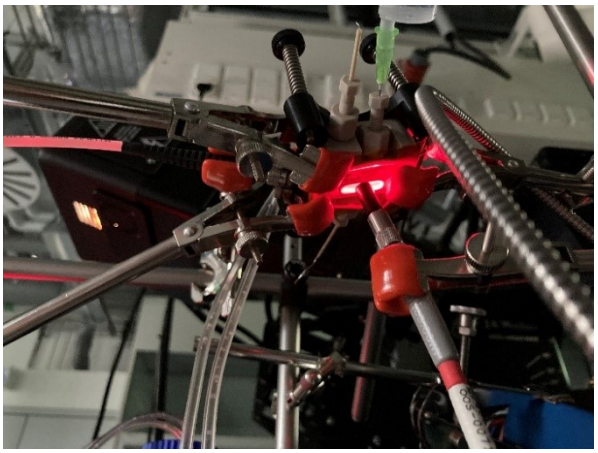

Supplementary Fig. S2. Spectral irradiance of the solar simulator and the UV LED measured at the working electrode position in the *in-situ* PEC cell filled with 0.5 M sulfuric acid using a spectrometer (left). The output of the fiber optic cable was attached to the entrance window of the *in-situ* PEC (right). For illustration purposes, a red LED was used here instead of the UV LED.

ALD process optimization for TiO_2

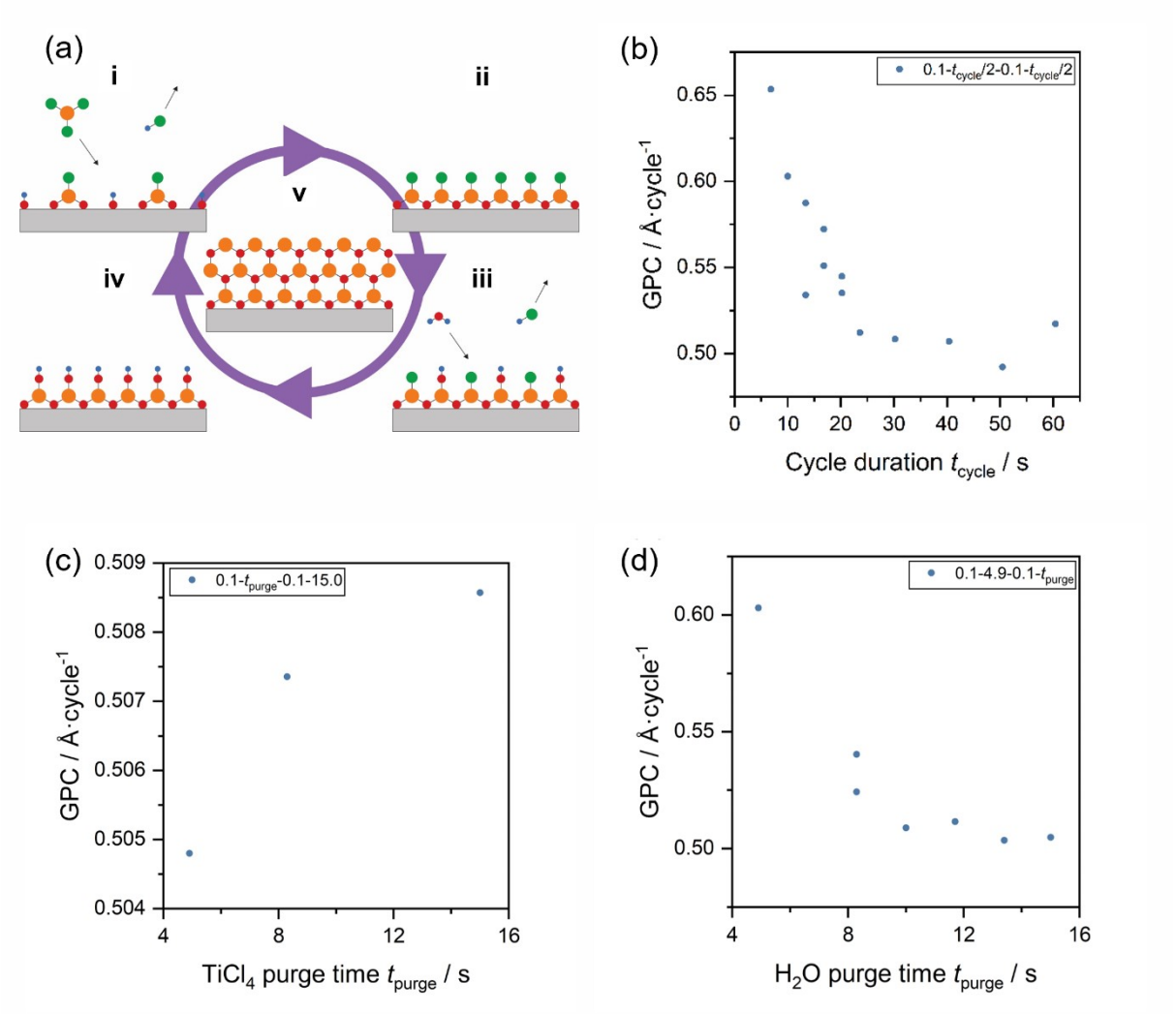

Supplementary Fig. S3. (a) Schematic illustration of an atomic layer deposition (ALD) cycle consisting of two half-cycles. i, iii: In the dosing steps, a precursor binds to all available surface sites. ii, iv: Excess precursor and volatile by-products are removed in purge and pump steps, leaving only a monolayer of precursor on the surface. The plots show the growth per ALD cycle (GPC) as a function of cycle duration (notation: precursor A pulse time / s - precursor A purge time / s - precursor B pulse time / s - precursor B purge time / s) for TiO_2 thin films on n^{++}-Si at 100 °C using titanium tetrachloride and water as precursors A and B (b). Optimization of the purge time with respect to minimum cycle duration at constant GPC for titanium tetrachloride $TiCl_4$ (c) and water (d) half-cycles.

Influence of synthesis temperature on crystallinity

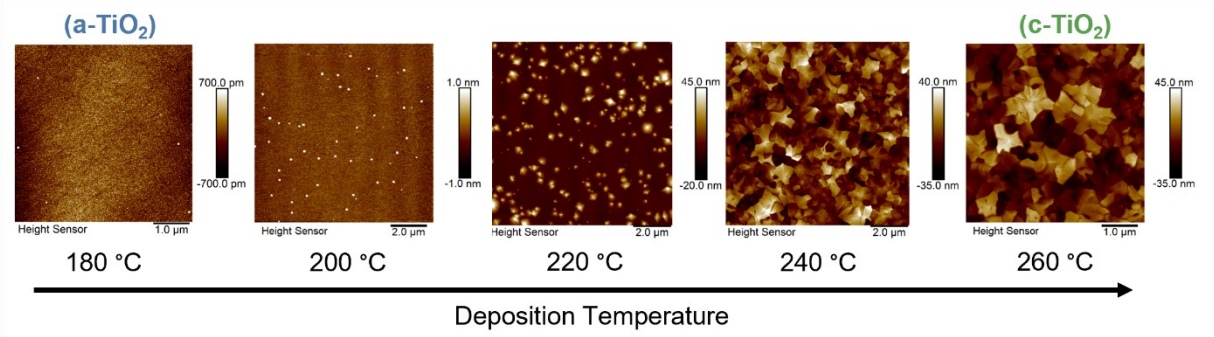

Supplementary Fig. S4. AFM surface morphology images of thermally ALD-grown TiO_2 thin films on $n^{++}Si$ with increasing deposition temperatures from 180 to 260 °C (2000 cycles). The color labels correspond to the samples discussed as model systems in the main text.

UV-Vis Spectroscopy

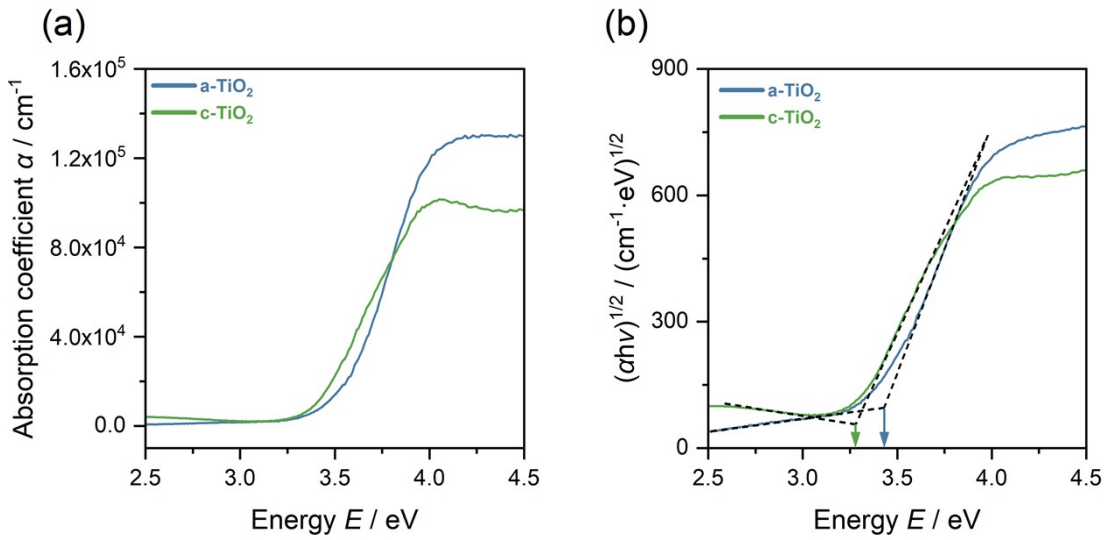

Supplementary Fig. S5. (a) Energy-dependent absorption coefficients derived from transmittance and reflectance spectra of ALD-grown TiO_2 films on quartz. (b) Corresponding Tauc plots for indirect allowed transitions. The optical bandgap energies determined by the two-line intersection method are approximately 3.28 eV for c-TiO_2, and 3.43 eV for a-TiO_2.

Chronoamperometry

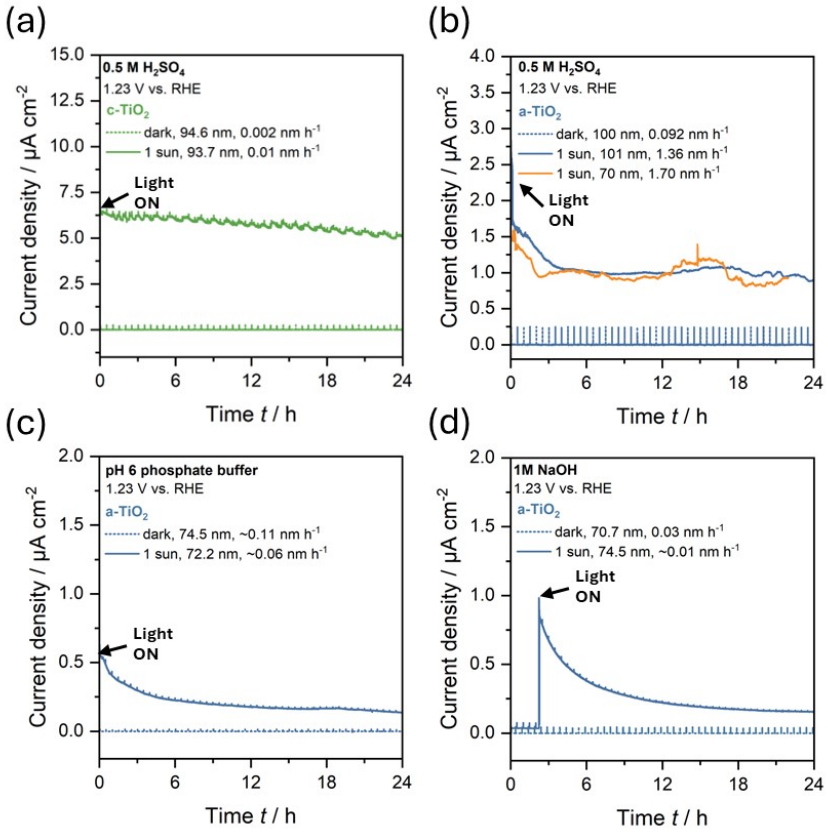

Supplementary Fig. S6. Chronoamperometry results for (a) c-TiO_2 under 0.5 M H_2SO_4, (b) a-TiO_2 under 0.5 M H_2SO_4, (c) a-TiO_2 under pH 6 phosphate buffer, and (d) a-TiO_2 under 1 M NaOH. The geometric area of the electrode exposed to the electrolyte in the *operando* SE cell is about 2.4 cm^2. The initial thickness of the films and the degradation rates determined by ellipsometry are shown in the corresponding legends. Brief measurement-induced perturbations in the current traces correspond to the periodic opening of the ellipsometer shutter (10 s every 30 min) for thickness acquisition. The crystalline c-TiO_2 exhibits the highest and most stable photocurrent in acidic medium. While a-TiO_2 shows higher photocurrents in acidic electrolyte compared to neutral and alkaline media, this increase coincides with significantly enhanced material loss. This behavior is consistent with partial consumption of photogenerated holes by photocorrosion in the amorphous phase. In contrast, c-TiO_2 maintains higher photocurrent with substantially lower degradation. For experiments conducted under illumination in acid and buffer, the light was switched on at the beginning of the measurement. In alkaline medium, illumination was introduced after 2.5 h, confirming the negligible influence of light on degradation under these conditions (see Fig. 4).

SE model

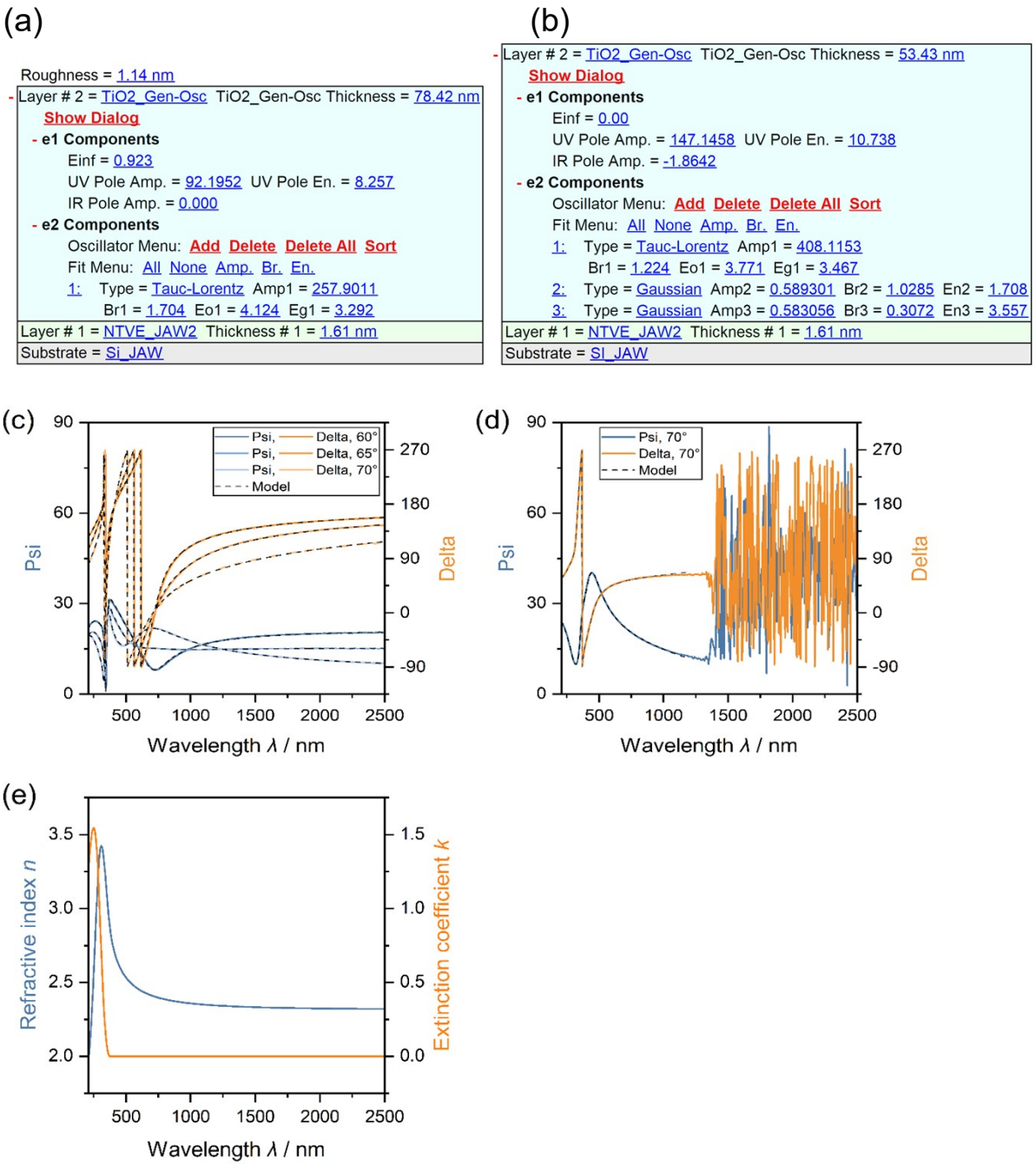

Supplementary Fig. S7. Example figures from CompleteEASE software (J.A. Woollam) showing the Tauc−Lorentz dispersion model for fitting the ALD-grown TiO_2 thin films on n^{++}-Si (a) in air and (b) in aqueous electrolyte, with two Gaussian oscillators added to the model. (c) Measured and modelled Psi and Delta values of TiO_2 films as a function of the wavelength at angles of incidence of 60°, 65° and 70° by *ex-situ* SE and (d) at a fixed incidence angle of 70° in the *in-situ* PEC filled with 0.5 M sulfuric acid. Note that for the *in-situ* measurements, the Psi and Delta values were only modelled in the wavelength range of 210−1200 nm due to absorption by the electrolyte. (e) Optical constants (refractive index n and extinction coefficient k) derived from the Tauc−Lorentz dispersion model for the TiO_2 layer.

Changes to the surface during PEC operation

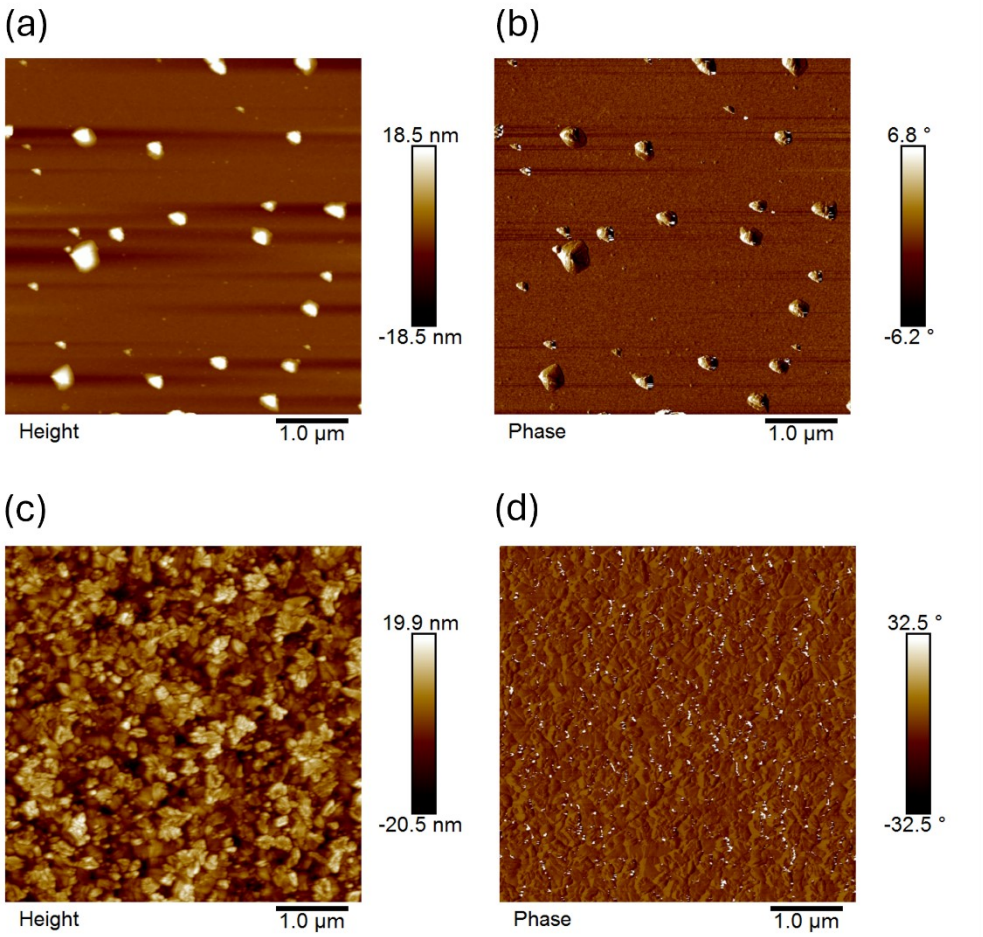

Supplementary Fig. S8. AFM topography scans of a-TiO_2 (a, b) and c-TiO_2 (c, d) after 72 h operation at 1.23 V vs. RHE in H_2SO_4 under 1 sun illumination (see Fig. 2 for topography of the pristine samples). For c-TiO_2, the overall thickness loss during operation was minimal. However, increased roughness at crystallite edges and the appearance of small surface particulates are observed, suggesting surface restructuring under operating conditions. In contrast, a-TiO_2 exhibits substantial material removal, with more than half of the initial thickness etched away. The images reveal exposed crystallites within the remaining matrix, consistent with preferential dissolution of the amorphous phase. Such behavior has been reported for thicker amorphous TiO_2 films, where interfacial effects at the SiOx substrate promote partial crystallization[1]. The emergence of this incipient crystallinity at reduced thickness may contribute to the observed decrease in photocorrosion rate below a certain thickness. Images were acquired using a Multimode 8 AFM (Bruker) at a scan rate of 0.3 Hz with an RTESPA probe (nominal spring constant 5 N/m, resonance frequency 150 kHz). A line-by-line least-squares polynomial fit was applied to correct background tilt.

Impedance spectroscopy

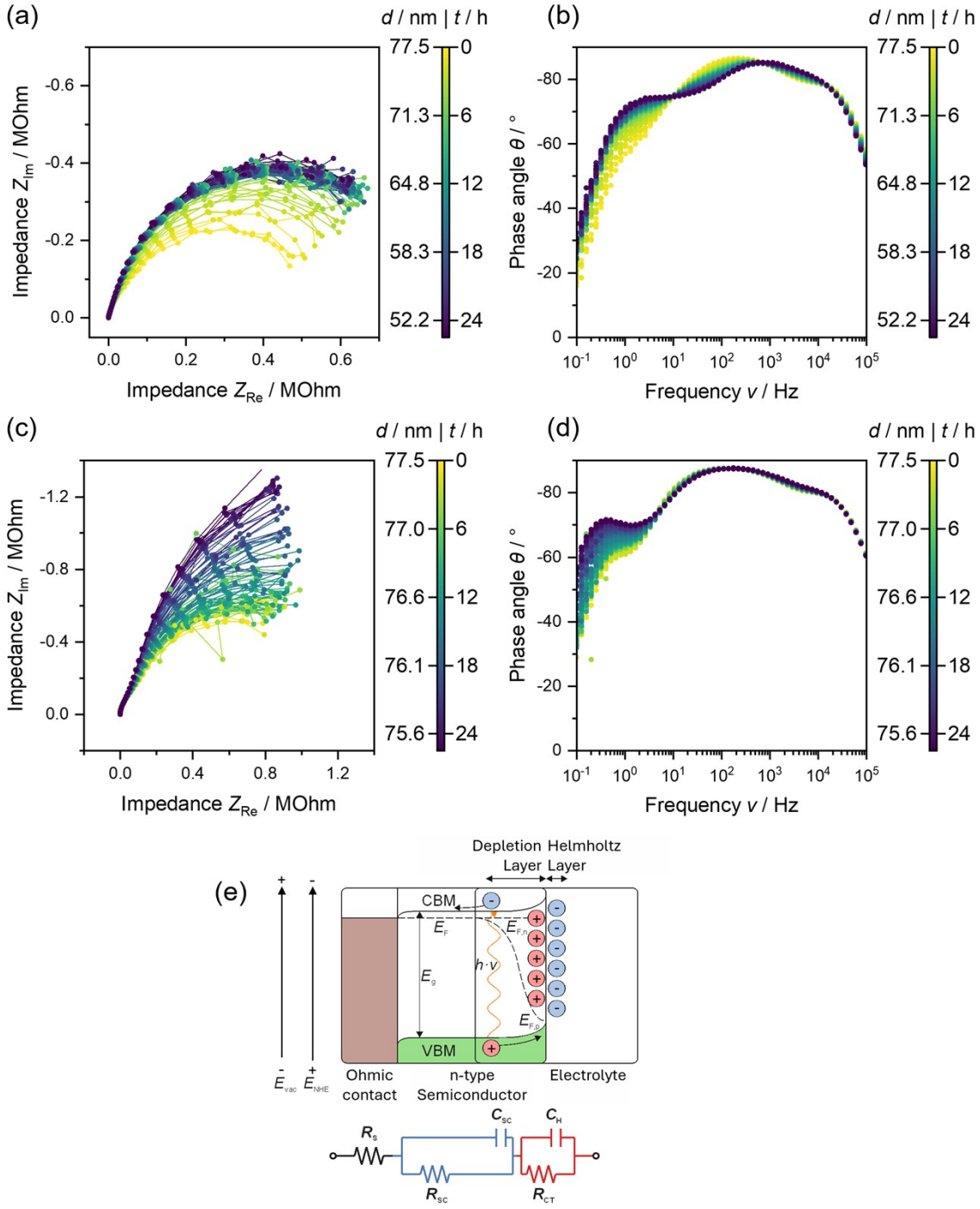

Supplementary Fig. S9. Electrochemical impedance spectroscopy (EIS) of the n^{++}Si/a-TiO_2 during PEC-operando degradation. Time and thickness dependent on (a) Nyquist plots and (b) Bode diagrams under illumination with 1 sun and (c) Nyquist plots and (d) Bode diagrams in the dark. (e) Energy diagram of an n-type semiconductor/electrolyte interface under steady-state illumination in quasi-static equilibrium, and corresponding electrochemical equivalent circuit used for fitting the EIS data. All measurements acquired at an applied DC potential of 1.23 V vs. RHE. EIS was acquired with a 25 mV AC amplitude perturbation and in the frequency range of 1 MHz−0.1 Hz.

1.